A soluble bone morphogenetic protein type IA receptor increases bone mass and bone strength

Marc Baud'huin[a,1], Nicolas Solban[b,1], Milton Cornwall-Brady[b], Dianne Sako[b], Yoshimi Kawamoto[b], Katia Liharska[b], Darren Lath[a], Mary L. Bouxsein[c], Kathryn W. Underwood[b], Jeffrey Ucran[b], Ravindra Kumar[b], Eileen Pobre[b], Asya Grinberg[b], Jasbir Seehra[b], Ernesto Canalis[d], R. Scott Pearsall[b,2], and Peter I. Croucher[a,e,2]

[a]Mellanby Centre for Bone Research, Department of Human Metabolism, University of Sheffield Medical School, Sheffield S10 2RX, United Kingdom; [b]Acceleron Pharma, Inc. Cambridge, MA 02139; [c]Orthopedic Biomechanics Laboratory, Beth Israel Deaconess Medical Center and Harvard Medical School, Boston, MA 02215; [d]Department of Research, St. Francis Hospital and Medical Center, Hartford, CT 06105; and [e]Garvan Institute for Medical Research, Sydney NSW 2010, Australia

Edited by Darwin J. Prockop, Texas A & M Health Science Center, Temple, TX, and approved June 1, 2012 (received for review April 2, 2012)

Diseases such as osteoporosis are associated with reduced bone mass. Therapies to prevent bone loss exist, but there are few that stimulate bone formation and restore bone mass. Bone morphogenetic proteins (BMPs) are members of the TGFβ superfamily, which act as pleiotropic regulators of skeletal organogenesis and bone homeostasis. Ablation of the BMPR1A receptor in osteoblasts increases bone mass, suggesting that inhibition of BMPR1A signaling may have therapeutic benefit. The aim of this study was to determine the skeletal effects of systemic administration of a soluble BMPR1A fusion protein (mBMPR1A–mFc) in vivo. mBMPR1A–mFc was shown to bind BMP2/4 specifically and with high affinity and prevent downstream signaling. mBMPR1A–mFc treatment of immature and mature mice increased bone mineral density, cortical thickness, trabecular bone volume, thickness and number, and decreased trabecular separation. The increase in bone mass was due to an early increase in osteoblast number and bone formation rate, mediated by a suppression of Dickkopf-1 expression. This was followed by a decrease in osteoclast number and eroded surface, which was associated with a decrease in receptor activator of NF-κB ligand (RANKL) production, an increase in osteoprotegerin expression, and a decrease in serum tartrate-resistant acid phosphatase (TRAP5b) concentration. mBMPR1A treatment also increased bone mass and strength in mice with bone loss due to estrogen deficiency. In conclusion, mBMPR1A–mFc stimulates osteoblastic bone formation and decreases bone resorption, which leads to an increase in bone mass, and offers a promising unique alternative for the treatment of bone-related disorders.

anabolic | therapy

Bone morphogenetic proteins (BMPs) are members of the TGF-β superfamily that were originally identified by their potent ectopic bone formation activity (1). BMPs regulate cell growth, differentiation, and function (2), and play an important role in regulating normal physiologic functions, although their precise role in bone remodeling remains unclear.

BMP signaling is mediated by activation of type I and type II serine-threonine kinase receptors. BMP ligands bind with high affinity to type I receptors followed by heterodimerization with type II receptors, allowing the type II receptor to phosphorylate a short stretch of amino acids in the type I receptor and activate a kinase activity. Activated BMP type I receptor phosphorylates immediate downstream targets, Smad1, Smad5, and Smad8 proteins, which interact with Smad4 and translocate to the nucleus to regulate target gene expression. BMPR1A (or ALK3) is a type I receptor that is known to have high affinity for BMP2 (3) and BMP4 (4), which are expressed in bone; however, the role of BMPR1A in the regulation of BMP2/4 function in the skeleton is unclear.

BMPs have potent osteogenic activity in vitro (5) and constitutive activation of BMPs, or exogenous application of BMPs, can induce ectopic bone formation in vivo (6, 7). *Bmpr1a* deletion in mice causes early embryonic lethality, before bone development, making the study of BMPR1A signaling in adult tissues difficult (8). Recently, conditional ablation of *Bmpr1a* has been used to study *Bmpr1a* disruption in osteoblasts (9). Mice with postnatal inactivation of *Bmpr1a* have an unexpected increase in bone mass (10), which is associated with decreased expression of the Wnt antagonists sclerostin (Sost) and dickkopf-1 (Dkk1) (11). Furthermore, conditional *Bmpr1a* disruption in osteoclasts also causes increased bone mass (12).

Recent studies have shown that mutations of ACVR1 (ALK2), a related BMP type I receptor, are associated with fibrodsyplasia ossificans progressive (FOP) (13, 14). FOP is a disease characterized by heterotopic ossification, suggesting that ACVR1 signaling may also be important in bone regulation. Conditional disruption of ACVR1 in osteoblasts also leads to an increase in bone mass due to decreases in Sost and Dkk1 expression (15).

BMPs induce osteogenesis, and BMP2 and BMP7 are approved therapies for treatment of nonunion fractures and spinal fusions (7, 16). However, BMP signaling in bone is complex (17, 18), and recent studies in cynomologous monkeys demonstrated that application of rhBMP2 in a core-defect model induces bone resorption before the stimulation of bone formation (19). Furthermore, the demonstration that disruption of signaling through BMPR1A in adult osteoblasts or osteoclasts (10, 12) increases bone mass provides evidence that alteration of the physiologic levels of BMPs and/or altering BMPR1A signaling may have positive effects on bone mass in vivo.

In this study, we developed a soluble mBMPR1A–mFc fusion protein, which binds with high affinity to BMP2 and BMP4 and prevents BMP signaling. mBMPR1A–mFc was administered by parenteral injection to gonadally intact immature and mature mice to study its effects on bone remodeling. It also was studied for its ability to influence bone loss induced by estrogen deficiency.

Results

Construction, Purification, and in Vitro Evaluation of mBMPR1A–mFc Fusion Protein. The extracellular domain of murine BMPR1A was cloned into pAID4 to produce the mBMPR1A–mFc construct (Fig. 1*A*). The construct was transfected into CHO cells and the

Author contributions: M.B., N.S., K.W.U., R.K., A.G., J.S., R.S.P., and P.I.C. designed research; M.B., N.S., M.C.-B., Y.K., K.L., D.L., M.L.B., E.P., A.G., and E.C. performed research; D.S. and J.U. contributed new reagents/analytic tools; M.B., N.S., M.C.-B., D.S., K.L., M.L.B., J.U., R.K., E.P., A.G., E.C., and R.S.P. analyzed data; and M.B., N.S., R.S.P., and P.I.C. wrote the paper.

Conflict of interest statement: N.S., M.C.-B., D.S., Y.K., K.L., K.W.U., J.U., R.K., E.P., A.G., J.S., R.S.P. are employees of Acceleron Pharma. P.I.C., M.L.B., and E.C. have received research funding from Acceleron Pharma.

This article is a PNAS Direct Submission.

[1]M.B. and N.S. contributed equally to this work.

[2]To whom correspondence may be addressed. E-mail: p.croucher@garvan.org.au or spearsall@acceleronpharma.com.

This article contains supporting information online at www.pnas.org/lookup/suppl/doi:10.1073/pnas.1204929109/-/DCSupplemental.

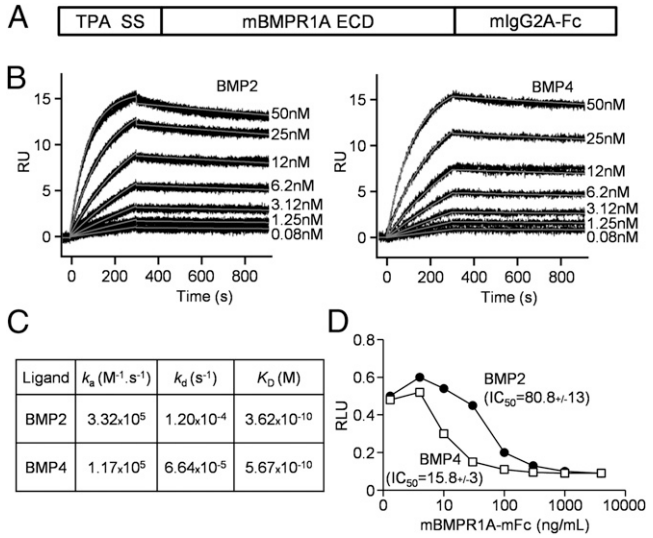

Ligand	k_a ($M^{-1}.s^{-1}$)	k_d (s^{-1})	K_D (M)
BMP2	3.32×10^5	1.20×10^{-4}	3.62×10^{-10}
BMP4	1.17×10^5	6.64×10^{-5}	5.67×10^{-10}

Fig. 1. Cloning and functional characterization of mBMPR1A–mFc. (*A*) Schematic representation of the mBMPR1A–mFc construct identifying the tissue plasminogen activator (TPA) signal sequence (SS), the murine BMPR1A extracellular domain (ECD) (residues Q24-R152), and the murine IgG2A–Fc domain (mIgG2A–Fc). (*B*) Kinetic analysis of BMP2 and BMP4 ligands binding to mBMPR1A–mFc performed on Biacore T100 at 20 °C. Antimurine Fc-specfic antibody was immobilized onto CM5 Biacore sensor chip using standard amino-coupling chemistry. mBMPR1A–mFc was captured on an antimurine Fc IgG flow cell at a density of ~100 relative units (RU). A concentration series of BMP2 and BMP4 (0.078–50 nM) was injected in duplicates over captured receptor and control flow cell at a flow rate of 50 μL/mL. Raw data (black lines) are overlaid with a global fit to a 1:1 model with mass transport term (red lines) obtained using BIAevaluation software. (*C*) Table summarizing kinetic parameters of BMP2 and BMP4 binding to mBMPR1A–mFc, where k_a = association rate constant, k_d = dissociation rate constant, and K_D = equilibrium dissociation constant. The equilibrium binding constant K_D was determined by the ratio of binding rate constants k_d/k_a. (*D*) Cell-based analysis of the ability of mBMPR1A–mFc to inhibit BMP2 and BMP4-induced signaling. Experimental sample values are expressed relative to control values and expressed as a ratio of relative luciferase units (RLU). The IC_{50} for each curve was calculated using SigmaPlot and represents the mean of three independent assays (mean ± SEM).

mBMPR1A–mFc fusion protein purified by sequential column chromatography. SDS/PAGE analysis identified a single protein band with a molecular mass of ~50 kDa under reducing and ~100 kDa under nonreducing conditions (Fig. S1*A*). SDS/PAGE and size exclusion chromatography showed that mBMPR1A–mFc was ~95% pure with no evidence of significant aggregation (Fig. S1*B*).

Surface plasmon resonance (SPR) was used to screen multiple TGFβ family ligands for binding to mBMPR1A–mFc. Of 29 different TGFβ superfamily ligands examined, BMP2 and BMP4 bound to mBMPR1A–mFc with high affinity (BMP2 = 0.362 nM and BMP4 = 0.567 nM) (Fig. 1 *B* and *C*). BMP6/7 and GDF5/6 also bound to mBMPR1A–mFc, but with up to 50-fold lower affinity. TGFβ1, TGFβ2, and TGFβ3 did not bind to mBMPR1A–mFc (Table S1).

To determine whether mBMPR1A–mFc prevented BMP2/BMP4 induction of SMAD signaling, a luciferase reporter assay was performed following transfection into T98G cells. Stimulation with BMP2 (12.8 ng/mL) or BMP4 (4 ng/mL) caused a five- to sixfold increase in luciferase activity, which was decreased in the presence of 10 and 100 ng/mL of mBMPR1A–mFc and completely blocked in the presence of 1 μg/mL mBMPR1A–mFc (Fig. 1*D*).

Blocking BMP2/4 Signaling Increases Bone Mass in Healthy Mice. To evaluate the skeletal response to inhibition of BMP2/BMP4 signaling with mBMPR1A–mFc, 12-wk-old female mice were treated with increasing concentrations of mBMPR1A–mFc. Treatment with mBMPR1A–mFc was associated with a greater increase in BMD (vs. baseline) than the vehicle-treated group ($P < 0.01$). After 6 wk of treatment, the increase of BMD in the 10 mg/kg group was 13.2% higher than the baseline level and was significantly different to the increase of the BMD in the vehicle-treated group (6.2%, $P < 0.001$, Fig. 2*A*).

Microcomputed tomography (μCT) analysis of the metaphyseal region of the proximal tibia showed greater trabecular bone volume in animals treated with mBMPR1A–mFc for 6 wk compared with vehicle-treated mice (Fig. 2*B*). The effect was dose dependent, with trabecular bone volume greater in mice treated with 1 mg/kg (131%), 3 mg/kg (208%,), and 10 mg/kg (346%, $P < 0.001$ for each) compared with controls (Fig. 2*C*). This increase in trabecular bone volume was due to higher trabecular number, (24.7 and 34.9% ($P < 0.01$), 57.9% ($P < 0.001$) (Fig. 2*D*), and trabecular thickness (17.2, 27.7, and 41.9%) with treatment with mBMPR1A–mFc at 1, 3, and 10 mg/kg, respectively, $P < 0.05$) (Fig. 2*E*). Cortical bone analysis showed an 8.3% and a 10.8% greater cortical thickness with mBMPR1A–mFc in the 3 mg/kg and the 10 mg/kg groups, respectively (Fig. 2*F*, $P < 0.05$).

Blocking BMP2/4 Signaling Increases Bone Mass as Early as 7 d Following Treatment. μCT analysis was used to determine whether short-term treatment with mBMPR1A–mFc increased bone mass (Fig. 3*A*). Quantitative analysis revealed higher trabecular BMD as early as 3 d of treatment (1.5%, $P < 0.05$) (Fig. 3*B*). Trabecular bone volume in the metaphyseal region of the proximal tibia was 38.1% higher than controls after 7 d of treatment with mBMPR1A–mFc (10 mg/kg), and 32.6 and 50.8% greater than controls ($P < 0.01$ for both) after 14 and 28 d of treatment, respectively (Fig. 3*C*). The increase in trabecular bone volume was associated with greater trabecular number and trabecular thickness and lower trabecular separation (Fig. 3 *D–F*). Similarly, trabecular bone mass in lumbar vertebra was significantly higher than controls after 7 d of treatment (Fig S2 *A–F*).

Blocking BMP2/4 Signaling with mBMPR1A–mFc Promotes an Early Increase in Osteoblast Number and Inhibits Dkk1 Expression in Osteoblasts. Histomorphometric analysis of trabecular bone in the proximal tibia following mBMPR1a–mFc treatment showed greater osteoblast number at day 3 (111%, $P < 0.05$), day 7 (70%, $P < 0.05$), day 14 (111%), and day 28 (47%) compared with vehicle-treated mice (Fig. 4 *A*, *i* and *B*). This difference decreased with time even though dosing continued. In separate studies using 12-wk-old mice, long-term mBMPR1A–mFc treatment (2, 4, or 6 wk) did not increase osteoblast number (Fig. 4*D*). In these studies mBMPR1A–mFc treatment was associated with a significant increase in mineralizing surface (weeks 2 and 4, $P < 0.05$) and bone formation rate after 4 wk ($P < 0.05$) compared with vehicle-treated animals (Table S2).

To understand the molecular mechanisms responsible for the early increase in osteoblast number, we examined the effect of mBMPR1A–mFc on BMP2 signaling and Dkk1 expression in osteoblasts. BMP2 treatment of SaOS2 cells increased Smads 1, 5, and 8 phosphorylation, and mBMPR1A–mFc treatment reduced the BMP2 effect (Fig. 5*A*). mBMPR1A–mFc decreased the expression of Dkk1 mRNA in osteoblasts (Fig. 5*B*). BMP2 treatment was associated with a concentration-dependent increase in Dkk1 protein production, which was prevented by mBMPR1A–mFc (Fig. 5*C*). Consistent with these data, Dkk1 levels in the serum of mBMPR1A–mFc-treated mice were decreased at day 14 compared with vehicle-treated mice (34.6 ± 2.3 vs. 23.8 ± 1.7, $P < 0.05$).

Blocking BMP2/4 Signaling with mBMPR1A–mFc Leads to a Late Decrease in Osteoclast Number and Inhibits Receptor Activator of NF-κB Ligand (RANKL) Expression in Osteoblasts. Histomorphometric analysis of trabecular bone in the proximal tibia showed a significant

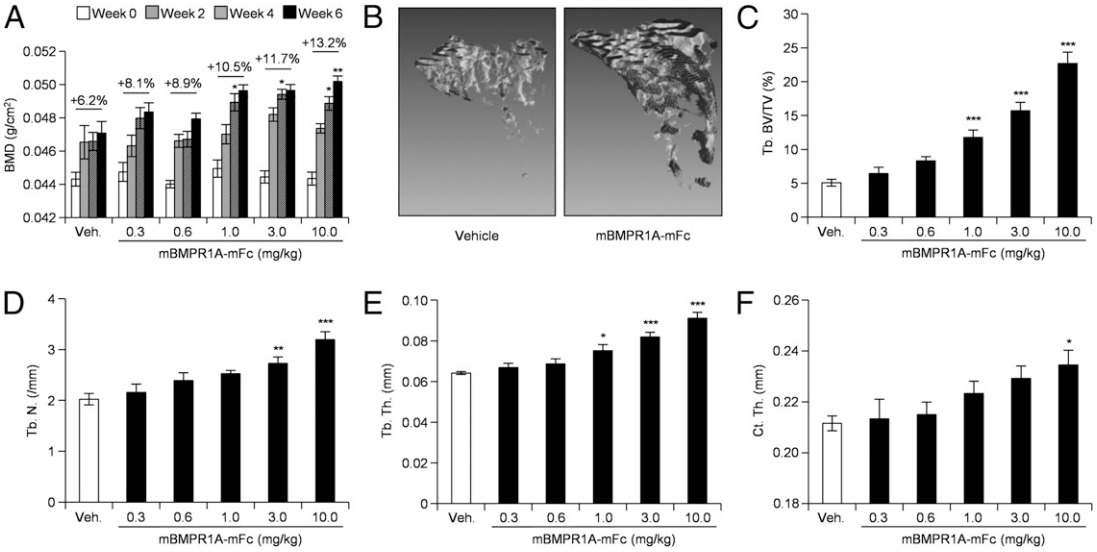

Fig. 2. mBMPR1A–mFc increases bone mass in healthy 12-wk-old mice. (*A*) Whole-body BMD, measured by DXA, of mice treated with mBMPR1A–mFc or vehicle (Veh) for 2, 4, or 6 wk. %, percentage of variation of the BMD between baseline and 6 wk of treatment. (*B*) Representative microCT images of the proximal tibia metaphysis, taken ex vivo, from mice treated with mBMPR1A–mFc (10 mg/kg) or vehicle (Veh) at 6 wk. (*C*–*E*) MicroCT analysis of the trabecular bone volume [BV/TV (%)] (*C*), trabecular number [Tb.N (/mm)] (*D*), and trabecular thickness [Tb.Th (mm)] (*E*) of the tibia of mice treated with increasing concentrations of mBMPR1A–mFc or vehicle at 6 wk. (*F*) MicroCT analysis of the cortical thickness [Ct.Th (mm)] in the tibia of mice treated with increasing concentrations of mBMPR1A–mFc or vehicle at 6 wk. Data represent mean ± SEM, $*P < 0.05$, $**P < 0.01$, $***P < 0.001$ compare with vehicle ($n = 6$ for each group).

decrease in osteoclast number (Oc.N) (Fig. 4*A*, *ii*). Oc.N was decreased at day 14 (41%, $P < 0.01$) and day 28 (63%, $P < 0.01$) compared with vehicle-treated mice (Fig. 4*C*). In a separate experiment, treatment with BMPR1A–mFc over 6 wk did not decrease osteoclast number (Fig. 4*E*). The decrease in osteoclast number was associated with a reduction in serum tartrate-resistant acid phosphatase (TRAP5b) levels in mBMPR1A–mFc-treated mice compared with vehicle-treated animals (67% at week 2, $P < 0.05$ and 56% at week 4) (Fig. 4*F*). These data suggest that there is a rapid, transient increase in bone formation associated with increased osteoblast number with a secondary effect of reduced osteoclast numbers and decreased resorption leading to increased bone mass.

To examine the molecular mechanisms responsible for the suppression of osteoclast number, we examined the effect of mBMPR1A–mFc on BMP2-induced RANKL and osteoprotegerin (OPG) expression in osteoblasts. mBMPR1A–mFc treatment caused a decrease in the expression of RANKL mRNA (41%, $P < 0.001$) (Fig. 6*A*) and a modest increase in OPG mRNA (16%, $P < 0.001$) in osteoblasts (Fig. 6*B*). RANKL serum levels were decreased after short-term treatment with mBMPR1A–mFc (16% at day 3, 23% at day 7, and 47% at day 14, $P < 0.05$, respectively) compared with vehicle-treated mice (Fig. 6*C*). This decrease of RANKL serum levels was sustained with mBMPR1A–mFc for up to 6 wk (57%, $P < 0.05$) (Fig. 6*E*). In contrast, serum OPG levels in mBMPR1A–mFc-treated mice were not increased in short-term (3 d and 14 d) treatment (Fig. 6*D*) but were increased with long-term treatment (36% at week 4 and 27% at week 6, $P < 0.01$ and $P < 0.05$, respectively) (Fig. 6*F*).

mBMPR1A–mFc Treatment Reverses Osteopenia in Ovariectomized (OVX) Mice. We next examined whether mBMPR1A–mFc could increase bone mass in ovariectomized mice with established bone loss. Total body and lumbar spine bone mineral density (BMD) were lower (6.9 and 24.6%, respectively), in ovariectomized mice compared with SHAM-operated animals ($P < 0.001$, Fig. 7 *A* and *B*). Treatment with mBMPR1A–mFc (10 mg/kg) was associated with a time-dependent increase in total body BMD compared with vehicle (VEH)-treated mice ($P < 0.0001$). Furthermore, SHAM-operated and OVX–VEH-treated mice maintained BMD similar to baseline levels during the study. Compared with baseline levels, OVX mice treated with mBMPR1A–mFc had a 5.8% increase in BMD at 2 wk and a 12.5% increase by 4 wk, which was maintained over 8 wk of treatment (Fig. 7 *A* and *B*). After 2 wk of treatment with mBMPR1A–mFc, BMD levels in OVX mice were comparable to those of SHAM-operated animals (Fig. 7 *A* and *B*). μCT analysis of the metaphyseal region of the proximal tibia confirmed the expected trabecular bone loss caused by ovariectomy (43% decrease compared with SHAM, Fig. 7*C*) before treatment. After 4 wk of treatment with mBMPR1A–mFc, trabecular bone volume was higher than OVX mice treated with vehicle (221%, $P < 0.001$) and SHAM-operated controls (53.8%, $P < 0.01$) (Fig. 7*C*). Greater effects were observed after 8 wk of treatment (+244% vs. VEH-treated OVX mice, +83.3% vs. SHAM controls, and +102.5% vs. baseline controls) (Fig. 7*C*). Cortical thickness at the tibial diaphysis was also higher in mBMPR1A–mFc-treated OVX mice compared with SHAM and baseline controls (+4.7% and +13.2%, respectively, Fig. 7*D*). These results show that mBMPR1A–mFc treatment reverses the osteopenia induced by ovariectomy.

mBMPR1A–mFc Treatment Increases Bone Strength in the Femur. To determine whether mBMPR1A–mFc also increased bone strength, three-point bending of the left femoral diaphysis was performed. Ovariectomy without treatment resulted in lower stiffness (13.3%, $P < 0.01$; Fig. 7*E*), maximum load (7.5%; Fig. 7*F*), and estimated Young's modulus (10.7%; Fig. 7*G*) compared with SHAM-operated control mice. mBMPR1A–mFc treatment of OVX mice resulted in greater bone strength, with a higher stiffness (13.7%, $P < 0.01$; Fig. 7*E*), maximum load (17.7%, $P < 0.01$; Fig. 7*F*), and estimated Young's modulus (36.4%, $P < 0.05$; Fig. 7*G*) compared with OVX–vehicle-treated mice.

Discussion

BMPR1A is expressed in most tissues throughout development and after birth (20, 21). Gene disruption of *Bmpr1a* results in embryonic lethality, making it difficult to use this model to investigate the role of BMPR1A in bone development, growth, and adult skeletal homeostasis (21). Conditional *Bmpr1a* ablation

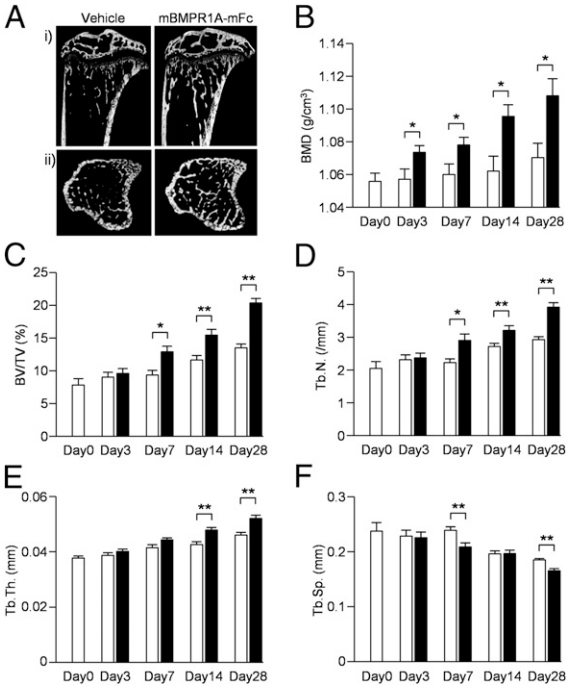

Fig. 3. mBMPR1A–mFc increases bone mass as early as 7 d following treatment. (*A*) Representative, longitudinal (*i*) and transverse (*ii*) microCT images of the proximal tibia metaphysis, taken ex vivo, from mice treated with mBMPR1A–mFc (10 mg/kg) or vehicle (Veh) for 7 d. (*B–F*) MicroCT analysis of trabecular bone mineral density [BMD (g/cm^3)] (*B*), trabecular bone volume [BV/TV (%)] (*C*), trabecular number [Tb.N (/mm)] (*D*), trabecular thickness [Tb. Th (mm)] (*E*), and trabecular separation [Tb.Sp (mm)] (*F*) of the tibia of mice treated with mBMPR1A–mFc (black bars) or vehicle (open bars) for 3 (n = 9), 7 (n = 8), 14 (n = 6), and 28 (n = 6) days. Data represent mean ± SEM, $*P < 0.05$, $**P < 0.01$, $***P < 0.001$ compare with vehicle by Student t test.

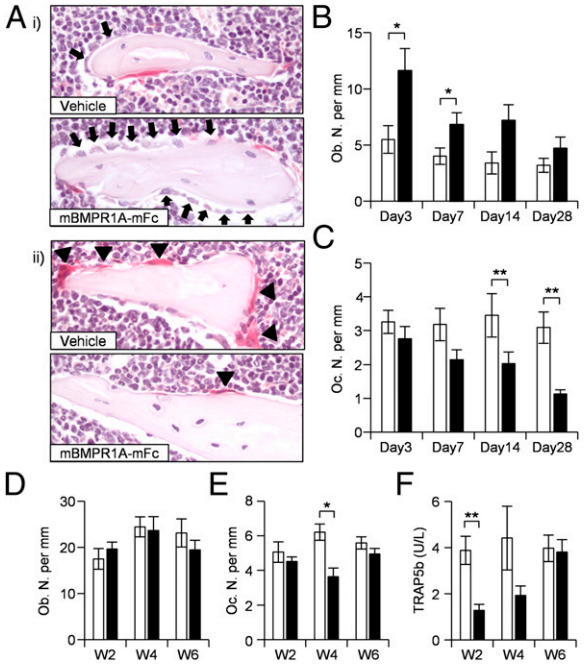

Fig. 4. mBMPR1A–mFc induces an early increase in osteoblast numbers followed by a decrease in osteoclast numbers. (*A*) Histological sections of the tibiae of mice treated with vehicle or mBMPR1A–mFc at day 7 (*i*) and day 28 (*ii*). Solid arrows identify osteoblasts and arrowheads identify TRAP$^+$ osteoclasts lining trabecular bone surfaces. (*B* and *C*) Histograms showing osteoblast number [Ob.N/BS (/mm)] (*B*) and osteoclast number [Oc.N/BS (/mm)] (*C*) in mice treated with vehicle (open bars) or mBMPR1A–mFc (black bars) for 3 (n = 9), 7 (n = 8), 14 (n = 6), and 28 (n = 6). (*D–F*) Histograms showing osteoblast number [Ob.N/BS (/mm)] (*D*) and osteoclast number [Oc.N/BS (/mm)] (*E*) in mice treated with vehicle or mBMPR1A–mFc for 2, 4, and 6 wk (n = 6). (*F*) Histogram showing serum TRAP5b concentration in mice treated with vehicle or mBMPR1A–mFc for 2, 4, and 6 wk. Data represent mean ± SEM $*P < 0.05$ and $**P < 0.01$ compared with vehicle by Student t test.

demonstrated that BMPR1A signaling plays a critical role in determining bone mass and raised the possibility that targeting this pathway may have therapeutic potential (9, 10, 12). In the present study we describe the development of a unique soluble BMPR1A fusion protein and investigated the ability of this protein to increase bone mass and strength in experimental models of osteoporosis.

Treatment with the mBMPR1A–mFc fusion protein resulted in a significant increase in bone mass in both young (7–10 wk) and old (14–18 wk) mice. The increased bone mass was associated with greater cortical thickness, trabecular width and number, and lower trabecular separation. An increase in BMD was seen as early as 3 d following start of treatment, with the increase in trabecular bone volume and number becoming apparent after 7 d. This is consistent with the recent demonstration that inducible osteoblast-specific *Bmpr1a* ablation increases bone mass in mice of 3 wk and 22 wk of age (10). Constitutive ablation of *Bmpr1a* in osteocalcin$^+$ cells also results in increased bone mass at 10 mo (9).

The increase in bone mass following mBMPR1A–mFc treatment was associated with an early increase in osteoblast number, the magnitude of which was reduced with time. This result suggests an effect of mBMPR1A–mFc on the latter stages of osteoblast differentiation and/or on mature osteoblasts, as opposed to effects on early stages of differentiation or on the mesenchymal stem cell pool when greater time may be required. Because osteoclast number was unchanged immediately after treatment the early increase in osteoblast numbers is likely to account for the rapid effect of mBMPR1A–mFc treatment on mass. Following long-term treatment (6 wk) osteoblast number returned to the level of vehicle-treated mice.

We also demonstrated that mBMPR1A–mFc, by blocking BMP2 signaling in osteoblasts, inhibited the expression of the soluble Wnt antagonist, Dkk1 (22, 23). Wnt signaling plays a critical role in regulating osteoblast differentiation and bone formation, and Dkk1 has been shown to be a negative regulator of Wnt signaling and osteoblast differentiation (24, 25). Indeed, BMP2 and BMP4 have been shown to induce Dkk1 expression during limb development in mice and chickens (26, 27). Although the demonstration that mBMPR1A–mFc decreases Dkk1 could account for the increase in osteoblast numbers and bone formation, the target population remains unclear. The speed of change would argue for an effect on more committed cells and whether Dkk1 may act on this population remains to be determined. These findings are supported by a recent study demonstrating that BMPR1A signaling regulates Dkk1 expression in osteoblasts (11). Although the relative contribution of Dkk1 inhibition to the early increase in osteoblasts is unclear, these data suggest that blocking BMP2/4 with mBMPR1A–mFc results in activation of downstream Wnt signaling in bone leading to an increase in bone mass.

In the present study, osteoclast numbers were not immediately affected by mBMPR1A–mFc treatment (3 d and 7 d). However, as treatment continued, the osteoclast number and serum TRAP5b concentrations were often decreased. This finding may be mediated indirectly via effects on osteoblasts or by direct effects on osteoclasts. In support of the former, we demonstrated that mBMPR1A–mFc blocked BMP2/4-induced signaling and up-regulated RANKL mRNA expression in osteoblasts in vitro, although it had little effect on OPG mRNA expression. Furthermore,

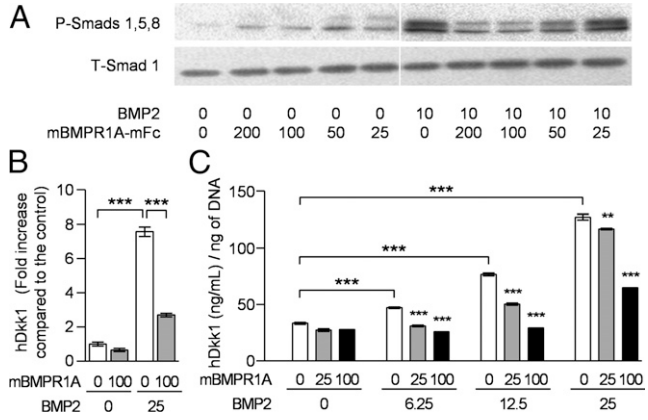

Fig. 5. mBMPR1A–mFc inhibits BMP2 signaling and decreases Dkk1 production in osteoblasts. (*A*) Western blot analysis of cell lysates, from SaOS2 treated with BMP2 and/or mBMPR1A–mFc illustrating the level of Phospho-SMADs (P-Smads) 1, 5, and 8. Total Smad1 (T-Smad1) confirm equal loading. (*B*) Quantitative RT-PCR analysis of the effect of BMPR1A–mFc on BMP2 induced Dkk1 mRNA expression in SaOS2 cells. (*C*) ELISA analysis of the effect of mBMPR1A–mFc on BMP2 induced Dkk1 protein production in the supernatant of SaOS2 cells. Data represent mean ± SEM for three experiments. Unless otherwise stated, $^{**}P < 0.01$ and $^{***}P < 0.001$ compared with control (no mBMPR1A–mFc).

mBMPR1A–mFc treatment decreased serum soluble RANKL and increased serum OPG concentrations. Similarly, overexpression of *Noggin*, an antagonist of BMP2 and BMP4 in osteoblasts, has been shown to reduce osteoclast number and osteoclastogenesis and increase bone mass (28). This observation is consistent

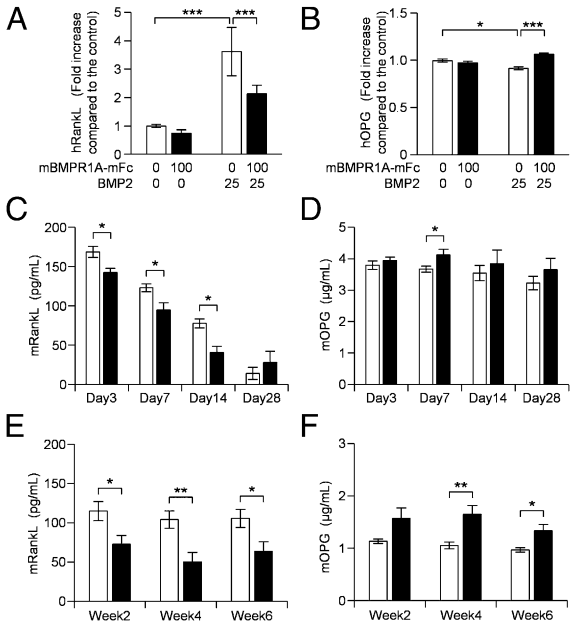

Fig. 6. mBMPR1A–mFc inhibits RANKL production in osteoblasts. (*A*) Quantitative RT-PCR analysis of the effect of mBMPR1A–mFc on BMP2 induced RANKL mRNA expression in SaOS2 cells. Data represent mean ± SEM for three experiments. (*B*) Quantitative RT-PCR analysis of the effect of mBMPR1A–mFc on OPG mRNA expression in SaOS2 cells. (*C* and *D*) Serum concentration of RANKL (*C*) and OPG (*D*) in mice treated with vehicle (open bars) or mBMPR1A–mFc (black bars) for 3 ($n = 9$), 7 ($n = 8$), 14 ($n = 6$), and 28 ($n = 6$). (*E* and *F*) Serum concentration of RANKL (*E*) and OPG (*F*) in mice treated with vehicle or mBMPR1A–mFc for 2, 4, and 6 wk ($n = 6$). $^{*}P < 0.05$, $^{**}P < 0.01$, and $^{***}P < 0.001$ compare with control. (*C*–*F*) Data were compared with their corresponding control by Student *t* test.

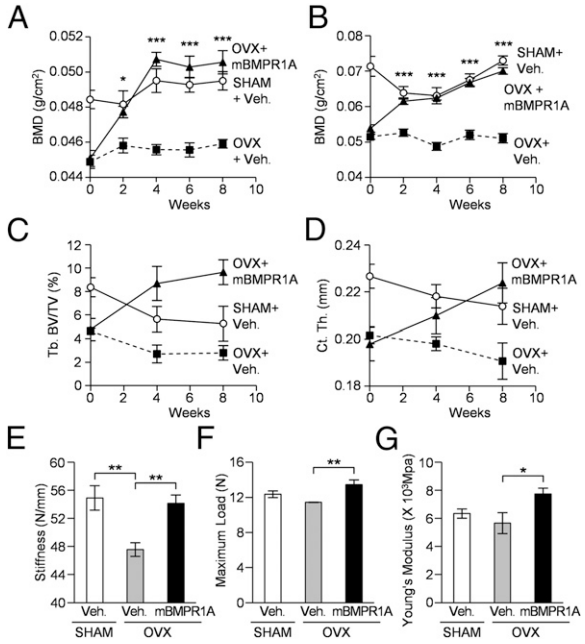

Fig. 7. mBMPR1A–mFc prevents ovariectomy-induced bone loss and improves bone strength. (*A* and *B*) Whole body (*A*) and lumbar vertebral (*B*) BMD measured in vivo by DXA biweekly of ovariectomized (OVX) mice treated with vehicle (Veh) or mBMPR1A–mFc (mBMPR1A) or SHAM-operated mice treated with vehicle. (*C* and *D*) Micro-CT analysis of Tb.BV/TV (*C*) and cortical thickness (*D*) in the proximal tibia metaphysis of OVX mice treated with vehicle or mBMPR1A–mFc or SHAM mice treated with vehicle. (*E*–*G*) Three-point bending analysis of stiffness (*E*), maximum load (*F*), and estimated Young's modulus (*G*) of the left femur of OVX mice treated with vehicle (gray bars) or mBMPR1A–mFc (black bars) or SHAM mice treated with vehicle (open bars). Data represent mean ± SEM $^{*}P < 0.05$ and $^{***}P < 0.001$ compared with OVX + vehicle ($n = 8$ for each group).

with the recent data of Noggin and Gremlin1 inactivation, which leads to osteopenia (29, 30).

Importantly, we not only found that mBMPR1A–mFc increased bone mass in normal healthy mice but we also demonstrated a positive effect in a model of estrogen-deficiency–induced bone loss. mBMPR1A–mFc treatment completely reversed the bone loss induced by OVX and restored both trabecular bone volume, number, and thickness and cortical thickness. Furthermore, mBMPR1A–mFc treatment restored bone biomechanical properties, demonstrating that bone architecture was also preserved.

In conclusion, short-term administration of mBMPR1A–mFc results in increases in bone mass, structure, and strength. Furthermore, we show that blocking the BMP2/4 signaling with a mBMPR1A–mFc can reverse the bone loss that occurs with estrogen deficiency. This robust response suggests that inhibition of signaling through BMPR1A with mBMPR1A–mFc represents a promising unique therapeutic approach for the treatment of bone-related disorders.

Materials and Methods

Expression, Purification, and Characterization of mBMPR1A–mIgG2a (mBMPR1A–mFc). The mouse BMPR1A extracellular domain (ECD) (Q24-R152) was obtained by PCR amplification, cloned into pAID4.UCOE (ubiquitin chromatin opening element) and transfected into CHO DU.K.X B11 cells. Conditioned medium containing mBMPR1A–mFc was purified using two-step column chromatography, dialyzed into PBS, and purity analyzed by SDS/PAGE. Aggregation was determined by size exclusion chromatography. Receptor-ligand binding affinities of mBMPR1A–mFc with TGFβ family ligands were determined by SPR. The effect of mBMPR1A–mFc on BMP signaling was determined using a cell-based luciferase gene reporter assay controlled by SMAD1/5/8 response element (see *SI Materials and Methods* for details).

Treatment of Mice with mBMPR1A–mFc. For short-term treatment studies, 6-wk-old C57BL/6 male mice were purchased from Harlan. Mice were treated with mBMPR1A–mFc (10 mg/kg) or vehicle (PBS) (n = 6), twice a week by i.p. injection and killed after 3 (n = 9), 7 (n = 8), 14 (n = 6), and 28 (n = 6) days of treatment. For long-term treatment studies, 12-wk-old C57BL/6 female mice were purchased from Taconic. Mice were treated with mBMPR1A–mFc (0.3, 0.6, 1.0, 3.0, or 10 mg/kg) or vehicle (PBS) (n = 6 for each group), twice a week by i.p. injection and killed after 2, 4, and 6 wk of treatment. For studies in a model of osteopenia, 8-wk-old female mice were ovariectomized (OVX) or SHAM-operated (SHAM), left untreated for 8 wk, and then treated with mBMPR1A–mFc (10 mg/kg) or vehicle (PBS) (n = 8 for each group), twice a week for 4 and 8 wk.

For dynamic bone histomorphometry, mice were injected with calcein (20 mg/kg) and demeclocycline (20 mg/kg) at 9 d and 2 d before sacrifice, or calcein at 6 d and 2 d before sacrifice. At sacrifice, the femurs, tibiae, and L4/5 vertebrae were collected for further analysis. All experiments were performed with the approval of Acceleron Pharma's Institutional Animal Care and Use Committee or under UK Home Office license, PPL40/3462.

Bone Densitometry and Analysis of Bone Structure. Whole-body bone mineral density was analyzed in vivo by dual-energy X-ray absorptiometry (DXA) (PIXImus). BMD and trabecular and cortical bone structural parameters in the femora, tibiae, and vertebrae was determined ex vivo by μCT according to published guidelines (31) (see *SI Materials and Methods* for details).

Biomechanical Testing. Biomechanical properties of the femur were determined by three-point bending, as described previously (32–34) (see *SI Materials and Methods* for details).

Bone Histomorphometric Analysis. Static or dynamic bone histomorphometry was performed on decalcified or undecalcified sections, respectively, from the femora or tibiae, as previously published (35, 36) (see *SI Materials and Methods* for details).

Serum Bone Biomarkers Measurements. Blood was collected by intracardiac puncture at sacrifice. Serum OPG, RANKL, Dkk1, and TRAP5b were measured using commercially available, species-specific Luminex antibody-immobilized microbead kits (Millipore) or ELISA kits (R&D Systems and IDS).

Western Immunoblot Analysis. Human SaOS-2 cells (a human osteosarcoma-derived osteoblast cell line) were treated for 20 min with BMP2 and/or mBMPR1A–mFc (preincubated for 1 h at 37 °C) and then lysed. Samples were fractionated, transferred to Immobilon-P membranes (Millipore) and incubated with antibodies to Phospho-SMADs 1/5/8 and Total-SMAD1. Labeled proteins were revealed using ECL reagent (see *SI Materials and Methods* for details).

Quantitative Real-Time PCR. RNA was isolated, using UltraSpec reagent (Biotecx), from SaOS2 cells cultured for 48 h with or without BMP2 (25 ng/mL; R&D Systems) in the presence or absence of mBMPR1A–mFc (100 ng/mL). cDNA was synthesized using the SuperScript System (Invitrogen). PCR reactions, data quantification, and analysis were performed according to the manufacturer's protocol (Applied Biosystems). Taqman primers and probes are described in *SI Materials and Methods*.

Dkk1 Measurement in Vitro. Supernatant were isolated from SaOS2 cells cultured for 72 h with or without BMP2 and in the presence or absence of mBMPR1A–mFc. Dkk1 protein level was measured by ELISA (R&D Systems). DNA content was quantified using Quant-iT PicoGreen dsDNA assay kit (Invitrogen). Dkk1 level was normalized to DNA content.

Statistical Analysis. Data were tested for normality using a Kolmogorov–Smirnov test. The mean ± SEM was calculated for all groups and compared by a two-tailed paired Student t test or by ANOVA, with the Dunnett's multiple comparisons test for post hoc analysis. Unless otherwise stated, multiple comparisons were performed by ANOVA. $P < 0.05$ was used as the criteria for statistical significance.

1. Wozney JM (1989) Bone morphogenetic proteins. *Prog Growth Factor Res* 1:267–280.
2. Massagué J (1992) Receptors for the TGF-beta family. *Cell* 69:1067–1070.
3. Keller S, Nickel J, Zhang JL, Sebald W, Mueller TD (2004) Molecular recognition of BMP-2 and BMP receptor IA. *Nat Struct Mol Biol* 11:481–488.
4. Hatta T, et al. (2000) Identification of the ligand-binding site of the BMP type IA receptor for BMP-4. *Biopolymers* 55:399–406.
5. Chen D, Zhao M, Mundy GR (2004) Bone morphogenetic proteins. *Growth Factors* 22: 233–241.
6. Kang Q, et al. (2004) Characterization of the distinct orthotopic bone-forming activity of 14 BMPs using recombinant adenovirus-mediated gene delivery. *Gene Ther* 11:1312–1320.
7. Gautschi OP, Frey SP, Zellweger R (2007) Bone morphogenetic proteins in clinical applications. *ANZ J Surg* 77:626–631.
8. Davis S, Miura S, Hill C, Mishina Y, Klingensmith J (2004) BMP receptor IA is required in the mammalian embryo for endodermal morphogenesis and ectodermal patterning. *Dev Biol* 270:47–63.
9. Mishina Y, et al. (2004) Bone morphogenetic protein type IA receptor signaling regulates postnatal osteoblast function and bone remodeling. *J Biol Chem* 279: 27560–27566.
10. Kamiya N, et al. (2008) Disruption of BMP signaling in osteoblasts through type IA receptor (BMPRIA) increases bone mass. *J Bone Miner Res* 23:2007–2017.
11. Kamiya N, et al. (2010) Wnt inhibitors Dkk1 and Sost are downstream targets of BMP signaling through the type IA receptor (BMPRIA) in osteoblasts. *J Bone Miner Res* 25: 200–210.
12. Okamoto M, et al. (2011) Conditional deletion of Bmpr1a in differentiated osteoclasts increases osteoblastic bone formation, increasing volume of remodeling bone in mice. *J Bone Miner Res* 26:2511–2522.
13. Fukuda T, et al. (2009) Constitutively activated ALK2 and increased SMAD1/5 cooperatively induce bone morphogenetic protein signaling in fibrodysplasia ossificans progressiva. *J Biol Chem* 284:7149–7156.
14. Shore EM, et al. (2006) A recurrent mutation in the BMP type I receptor ACVR1 causes inherited and sporadic fibrodysplasia ossificans progressiva. *Nat Genet* 38:525–527.
15. Kamiya N, Kaartinen VM, Mishina Y (2011) Loss-of-function of ACVR1 in osteoblasts increases bone mass and activates canonical Wnt signaling through suppression of Wnt inhibitors SOST and DKK1. *Biochem Biophys Res Commun* 414:326–330.
16. Wingerter S, Tucci M, Bumgardner J, Benghuzzi H (2007) Evaluation of short-term healing following sustained delivery of osteoinductive agents in a rat femur drill defect model. *Biomed Sci Instrum* 43:188–193.
17. Winnier G, Blessing M, Labosky PA, Hogan BL (1995) Bone morphogenetic protein-4 is required for mesoderm formation and patterning in the mouse. *Genes Dev* 9:2105–2116.
18. Zhang H, Bradley A (1996) Mice deficient for BMP2 are nonviable and have defects in amnion/chorion and cardiac development. *Development* 122:2977–2986.
19. Seeherman HJ, Li XJ, Bouxsein ML, Wozney JM (2010) rhBMP-2 induces transient bone resorption followed by bone formation in a nonhuman primate core-defect model. *J Bone Joint Surg Am* 92:411–426.
20. Dewulf N, et al. (1995) Distinct spatial and temporal expression patterns of two type I receptors for bone morphogenetic proteins during mouse embryogenesis. *Endocrinology* 136:2652–2663.
21. Mishina Y, Suzuki A, Ueno N, Behringer RR (1995) Bmpr encodes a type I bone morphogenetic protein receptor that is essential for gastrulation during mouse embryogenesis. *Genes Dev* 9:3027–3037.
22. Mao B, et al. (2001) LDL-receptor-related protein 6 is a receptor for Dickkopf proteins. *Nature* 411:321–325.
23. Brott BK, Sokol SY (2002) Regulation of Wnt/LRP signaling by distinct domains of Dickkopf proteins. *Mol Cell Biol* 22:6100–6110.
24. Tian E, et al. (2003) The role of the Wnt-signaling antagonist DKK1 in the development of osteolytic lesions in multiple myeloma. *N Engl J Med* 349:2483–2494.
25. Fujita K, Janz S (2007) Attenuation of WNT signaling by DKK-1 and -2 regulates BMP2-induced osteoblast differentiation and expression of OPG, RANKL and M-CSF. *Mol Cancer* 6:71.
26. Mukhopadhyay M, et al. (2001) Dickkopf1 is required for embryonic head induction and limb morphogenesis in the mouse. *Dev Cell* 1:423–434.
27. Grotewold L, Rüther U (2002) The Wnt antagonist Dickkopf-1 is regulated by Bmp signaling and c-Jun and modulates programmed cell death. *EMBO J* 21:966–975.
28. Okamoto M, Murai J, Yoshikawa H, Tsumaki N (2006) Bone morphogenetic proteins in bone stimulate osteoclasts and osteoblasts during bone development. *J Bone Miner Res* 21:1022–1033.
29. Canalis E, Parker K, Zanotti S (2012) Gremlin1 is required for skeletal development and postnatal skeletal homeostasis. *J Cell Physiol* 227:269–277.
30. Canalis E, Brunet LJ, Parker K, Zanotti S (2012) Conditional inactivation of noggin in the postnatal skeleton causes osteopenia. *Endocrinology* 153:1616–1626.
31. Bouxsein ML, et al. (2010) Guidelines for assessment of bone microstructure in rodents using micro-computed tomography. *J Bone Miner Res* 25:1468–1486.
32. Glatt V, Canalis E, Stadmeyer L, Bouxsein ML (2007) Age-related changes in trabecular architecture differ in female and male C57BL/6J mice. *J Bone Miner Res* 22:1197–1207.
33. Leung CK, Lam FK (1996) Performance analysis for a class of iterative image thresholding algorithms. *Pattern Recognit* 29:1523–1530.
34. Ridler TW, Calvard S (1978) Picture thresholding using an iterative selection method. *IEEE Trans Syst Man Cybern* 8:630–632.
35. Heath DJ, et al. (2009) Inhibiting Dickkopf-1 (Dkk1) removes suppression of bone formation and prevents the development of osteolytic bone disease in multiple myeloma. *J Bone Miner Res* 24:425–436.
36. Pearsall RS, et al. (2008) A soluble activin type IIA receptor induces bone formation and improves skeletal integrity. *Proc Natl Acad Sci USA* 105:7082–7087.